Exceptionally High Geothermal Heat Flux Needed to Sustain the Northeast Greenland Ice Stream

Silje Smith-Johnsen[1], Basile de Fleurian[1], Nicole Schlegel[2], Helene Seroussi[2], and Kerim Nisancioglu[1,3]

[1]Department of Earth Science, University of Bergen, Bjerknes Centre for Climate Research, Norway
[2]Jet Propulsion Laboratory, California Institute of Technology, Pasadena, California, USA
[3]Centre for Earth Evolution and Dynamics, University of Oslo, Oslo, Norway

Correspondence: Silje Smith-Johnsen (silje.johnsen@uib.no)

Abstract. The Northeast Greenland Ice Stream (NEGIS) currently drains more than 10% of the Greenland Ice Sheet area, and has recently undergone significant dynamic changes. It is therefore critical to accurately represent this feature when assessing the future contribution of Greenland to sea level rise. At present, NEGIS is reproduced in ice sheet models by inferring basal conditions using observed surface velocities. This approach helps estimate conditions at the base of the ice sheet, but cannot

5 be used to estimate the evolution of basal drag in time, so it is not a good representation of the evolution of the ice sheet in future climate warming scenarios. NEGIS is suggested to be initiated by a geothermal heat flux anomaly close to the ice divide, left behind by the movement of Greenland over the Icelandic plume. However, the heat flux underneath the ice sheet is largely unknown, except for a few direct measurements from deep ice core drill sites. Using the Ice Sheet System Model (ISSM), with ice dynamics coupled to a subglacial hydrology model, we investigate the possibility of initiating NEGIS by inserting hotspots

10 with various locations and intensities. We find that a minimum geothermal heat flux value of $970 \ mW/m^2$ located close to EastGRIP is required locally to reproduce the observed NEGIS velocities, consistent with previous estimates. By including high geothermal heat flux and the effect of water on sliding, we successfully reproduce the main characteristics of NEGIS in an ice sheet model without using data assimilation.

1 Introduction

15 The Greenland Ice Sheet (GrIS) displays large spatial variations in surface velocity, with a few fast-flowing outlets draining most of the interior (Rignot and Mouginot, 2012). It is therefore critical to capture the complex flow pattern of GrIS in models used for future sea level projections. Recent developments in ice sheet models such as efficient parallel computation (Khroulev and PISM-Authors, 2015), better representation of flow equations (Larour et al., 2012), detailed basal topography (Morlighem et al., 2014) and the inclusion of subglacial hydrology have contributed to greatly improve the representation of this spatially

20 varying flow (Aschwanden et al., 2016). In addition to these advances, inversion for basal friction using surface velocities has proved to be a powerful tool (Morlighem et al., 2013), and models are now able to capture most of the complex flow pattern of the ice sheet. Inversions are useful to capture present day velocity, but mask information that are needed to evolve these conditions in time. Therefore, we cannot fully rely on inversions for future projections, as basal conditions may evolve as a result of a changing climate and in turn influence ice dynamics.

25   The Northeast Greenland Ice Stream (NEGIS) drains more than 10 % of GrIS and is exceptional by displaying high velocities all the way to the ice divide (Rignot and Mouginot, 2012). Despite its large impact on the GrIS mass balance, NEGIS is not accurately represented in ice sheet models without inverting for basal friction (Goelzer et al., 2018). Aschwanden et al. (2016) simulated NEGIS in the Parallel Ice Sheet Model, capturing high velocities using a simple hydrology model, however, lacking the far inland onset of the ice stream. Beyer et al. (2018) used the basal melt rates from the model by Aschwanden et al.

30   (2016) in a more sophisticated hydrology model to reproduce NEGIS in the Ice Sheet System Model (ISSM). They capture the high velocity flow of the outlets well, but the representation of the transition areas outside of the main trunk are more diffuse compared to the observed values. These studies illustrate how we are getting closer to reproducing present day NEGIS in ice sheet models. However, the characteristic clearly defined shear margins and high velocities upstream at the onset of the ice stream are still lacking.

35   To understand why high upstream velocities are not reproduced in models, one must look into how the ice stream is initiated. The origin of NEGIS has been explained by a geothermal heat flux (GHF) anomaly left behind by the passage of the Icelandic plume (Fahnestock et al., 2001; Rogozhina et al., 2016; Martos et al., 2018; Alley et al., 2019). Interpretation of radar data points to unusually high basal melt rates at the head of the ice stream, corresponding to an exceptionally high geothermal heat flux of 970 mW/m^2 (Fahnestock et al., 2001; Macgregor et al., 2016; Alley et al., 2019). A local increase in GHF intensifies

40   basal water production and potentially enhances basal sliding (Smith-Johnsen et al., in reviewa). Unfortunately, geothermal heat flux maps for Greenland display a large spread of values (Rogozhina et al., 2012; Shapiro and Ritzwoller, 2004; Fox Maule et al., 2009; Martos et al., 2018; Rogozhina et al., 2016; Greve, 2019). These large uncertainties in the estimates of the GHF have been shown to dominate the uncertainty on the ice flux in this region (Smith-Johnsen et al., in reviewb). In addition, the GHF maps are coarse and may not capture local anomalies like the one suggested to exist at the head of NEGIS (Fahnestock

45   et al., 2001; Macgregor et al., 2016; Alley et al., 2019). Accurately capturing such a feature and explicitly representing the effect of high melt rates on basal sliding, is key to reproduce the distinct velocity pattern of NEGIS in ice sheet models.

Here, we study the impact of the presence and intensity of a mantle plume at the head of NEGIS on the ice flow structure. We use a sophisticated hydrology model (de Fleurian et al., 2014, 2016) coupled to ice dynamics in the Ice Sheet System Model (ISSM; Larour et al., 2012) to capture the influence of enhanced basal melt on ice dynamics. We first describe the models and

50   different plume experiments. Finally, we present and discuss resulting basal conditions and surface velocities corresponding to the various plume configurations.

2   Methods

2.1   Ice Flow Model

To simulate the NEGIS ice flow, we apply the model configuration from Schlegel et al. (2013, 2015) further developed and

55   adapted by (Smith-Johnsen et al., in reviewb). We use the Ice Sheet System Model (Larour et al., 2012), a 3D thermomechanical ice flow model, and explicitly represent the effect of high melt rates on subglacial hydrology (de Fleurian et al., 2014, 2016), which provides the effective pressure (N, the difference between ice overburden pressure and water pressure at the bed) that

Table 1. Definitions and values of variables in the subglacial hydrology model

Description	Unit	Value
effective pressure	Pa	
compressibility of water	Pa^{-1}	5.04e-10
leakage factor	m	1e-09
inefficient compressibility	Pa^{-1}	1e-08
inefficient porosity		0.4
inefficient thickness	m	20
inefficient transmitivity	m^2/s	0.002
efficient compressibility	Pa^{-1}	1e-08
efficient porosity		0.4
efficient initial thickness	m	0.005
efficient collapsing thickness	m	8e-05
efficient maximal thickness	m	5
efficient conductivity	m^2/s	25

controls basal sliding through a linear friction law (Cuffey and Paterson, 2010):

$$\tau_b = -\alpha^2 N \mathbf{v}_b \tag{1}$$

60 where τ_b is the basal drag, α basal friction coefficient, N effective pressure, and $\mathbf{v}_b$ the basal velocity. The hydrology model takes the basal melt rates as input, and computes the effective pressure. Nodes with no basal melt are given an effective pressure equal to the ice overburden pressure. The hydrology model consists of two porous sediment layers, representing the inefficient and efficient drainage system. The efficient drainage system is activated when N reaches zero, and may be deactivated as the water is evacuated and N increases again. Definitions and values of variables in the subglacial hydrology model are given in

65 Table 1. The hydrology model and its implementation in ISSM are described in detail in de Fleurian et al. (2014, 2016).

For the thermal model we rely on the enthalpy formulation by Aschwanden et al. (2012), implemented in ISSM (Seroussi et al., 2013) with surface temperatures from Ettema et al. (2009) and geothermal heat flux from Fox Maule et al. (2009). In addition we use a mantle plume module in ISSM to create elevated geothermal heat flux anomalies (Seroussi et al., 2017). Basal topography is from BedMachine (Morlighem et al., 2014) (Figure 1a) and we apply submarine melt rates under the

70 floating ice (Rignot et al., 2001). For the stress balance equation, we use a 3D Higher-Order approximation (Pattyn, 2003). Our model domain consists of 9974 horizontal elements, ranging from 1 km in areas with high velocity gradients to a maximum of 15 km at the ice divide (Figure 1b). We use linear P1 elements to solve the stress balance equations and quadratic P2 elements for the thermal analysis, in order to capture sharp temperature gradients, despite using only 5 layers (Cuzzone et al., 2018).

We aim to represent the observed NEGIS velocity pattern in an ice sheet model without inverting for the basal friction

75 coefficient. However, to initialize the hydrology model, we do simulate the present day ice stream by inferring basal friction
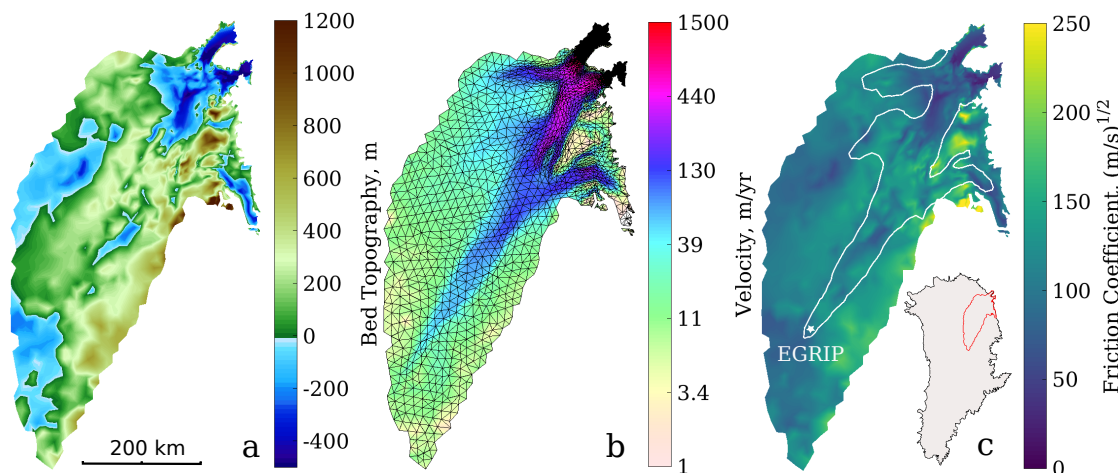
Figure 1. (a) bed topography from BedMachine (Morlighem et al., 2014) interpolated onto the model mesh, (b) InSAR-derived surface velocities (Rignot and Mouginot, 2012) and anisotropic model mesh refined in areas with high velocity gradients, (c) friction coefficient as a linear function of bed topography (Eq. 2) used in Eq. 1. The white contour shows the area of the NEGIS with observed surface velocity of 50 m/yr and the star shows the position of the East Greenland Ice-Core Project (EGRIP). The inset map in the lower right corner shows Greenland with the model domain outlined in red.

from present-day velocities (Figure 1b). The basal melt rates from this simulation are used to initialize the subglacial hydrology model, which we run for 150 years in order to reach an equilibrium in terms of water pressure. The resulting effective pressure field computed by the hydrology model, N, is used in the friction law (Eq.1), and kept constant in time. Finally, we run a 4 kyr simulation with the basal condition generated by the hydrology model to provide steady state surface velocities. Note that we do not use the friction coefficient, α, from the inversion in the forward ice flow simulation, as it is only used to initialize the subglacial hydrology model.

Previous modelling studies lack sharp velocity gradients defining NEGIS (Aschwanden et al., 2016; Beyer et al., 2018). To capture this we let the basal friction coefficient, α, depend linearly on the bed elevation using the following equation:

$$\alpha = min(max(1, 0.13 * bed + 100), 250) \tag{2}$$

where 100 $(m/s)^{1/2}$ is the mean value of the inversion alpha used in (Smith-Johnsen et al., in reviewb), and we cap the values between 1 and 250 $(m/s)^{1/2}$. 0.13 is tuned to approximately match the observed velocities at the grounding line of 79N. The resulting friction coefficient, α, is shown in Figure 1c. We argue that low lying topography will have more marine sediments, and thus a softer and less resistive bed, allowing high velocities of the outlet glaciers. A similar approach with basal shear stress defined as a function of bed elevation was previously used by Åkesson et al. (2018) and by Aschwanden et al. (2016). Our simple friction relationship is supported by observations, as bed topography roughness for the NEGIS region shows a pattern inversely correlated with bed elevation (Cooper et al., 2019).

Table 2. Mantle Plume parameter overview for the plume experiments

Parameter	Description	Value	Unit
mantleconductivity	mantle heat conductivity	2.5	W/m^3
nusselt	nusselt number, ratio of mantle to plume	500000	
dtbg	background temperature gradient	0.013	$degree/m$
plumeradius	radius of the mantle plume	varying	m
topplumedepth	depth of the mantle plume top below the crust	5000	m
bottomplumedepth	depth of the mantle plume base below the crust	varying	km
crustthickness	thickness of the crust	1	m
uppercrustthickness	thickness of the upper crust	1	m
uppercrustheat	volumic heat of the upper crust	$1.33e - 06$	W/m^3
lowercrustheat	volumic heat of the lower crust	$2.7e - 07$	W/m^3

Table 3. Overview of mantle plume parameters, modelled GHF and friction parameters.

Simulation	Position	Radius (km)	Depth (km)	max GHF (mW/m^2)	$\alpha\ ((m/s)^{1/2})$	N (MPa)
Ctrl	no plume	no plume	no plume	no plume	varying	modelled
plume970	center	50	5000	970	varying	modelled
plume677	center	50	3000	677	varying	modelled
plume836	center	50	4000	836	varying	modelled
plume909	center	50	4500	909	varying	modelled
plume970SW	SW	50	5000	970	varying	modelled
plume970SE	SE	50	5000	970	varying	modelled
plume970NE	NE	50	5000	970	varying	modelled
plume970NW	NW	50	5000	970	varying	modelled
plume494	center	300	3000	494	varying	modelled
plume594	center	200	2500	594	varying	modelled
plume775	center	100	2000	775	varying	modelled
plume792	center	200	3000	792	varying	modelled
noHydro	no plume	no plume	no plume	no plume	varying	approximated
Ctrl-uni	no plume	no plume	no plume	no plume	90	modelled
plume970-uni	center	50	5000	970	90	modelled

2.2 Experiments

In order to capture the high upstream velocity of NEGIS, we alter the geothermal heat flux by simulating a range of mantle
plumes close to the head of the ice stream, at the onset of fast flow (Seroussi et al., 2017). The mantle plume module in
ISSM computes the geothermal heat flux, given the plume parameters in Table 2, and the maximum GHF values range from

494 to 970 mW/m^2. To disentangle the effect of the mantle plume we run a Ctrl simulation without a mantle plume, using only the geothermal heat flux from Fox Maule et al. (2009). This GHF map is ranging from 40 mW/m^2 in the north-west to 77 mW/m^2 in the north-east below the Storstrømmen outlet, with an average value of 54 mW/m^2.

100   In our main experiment, plume970, the plume parameters were chosen to generate a GHF anomaly coherent with the one hypothesized by Fahnestock et al. (2001) and Macgregor et al. (2016). The resulting GHF anomaly is $\sim 50\ km$ in diameter with a maximum GHF value of 970 mW/m^2 (Table 3), and we position it directly underneath the EGRIP deep ice core drilling site (Figure 1c).

    To determine the minimum geothermal heat flux needed to initiate the onset of NEGIS close to the ice divide, we compute

105   three alternative plume configurations with lower intensity. We obtain the lower geothermal heat flux by decreasing the bottom plume depth parameter to 4500, 4000 and 3000 km for simulation plume909, plume836 and plume677, respectively (Table 3). Additionally, we compute four plume configurations where we change the position of the plume. We move the plume970 75 km to the south-west, south-east, north-east and north-west in the plume970SW, plume970SE, plume970NE, plume970NW experiments, respectively (Table 3). To investigate the influence of the area of the mantle plume, we compute four plume

110   configurations with larger area, compensated for by a smaller heat flux. To obtain this we increase the plume radius to values of 100-300 km, and decrease the bottom plume depth to values of 2000-3000 km, resulting in the experiments plume494, plume594, plume775 and plume792 (Table 3).

    Finally, to investigate the influence of our friction coefficient distribution, we run three additional simulations. First, we run a simulation without modelled effective pressure, but instead using effective pressure approximated to hydrostatic pressure,

115   commonly used in ISSM (no Hydro, Table 3). Then we run two simulations with a uniform friction of $\alpha = 90\ (m/s)^{1/2}$; one without a plume (Ctrl-uni, Table 3) and one with the 970 mW/m^2 plume (plume970-uni, Table 3).

3   Results

In the Ctrl simulation we use the geothermal heat flux from Fox Maule et al. (2009) (Figure 2a), with a value of 54 mW/m^2 at the onset of the ice stream. We run a steady state solution to retrieve the basal melt rates, as shown in Figure 2f. Melt rates

120   at the head of the ice stream (at EGRIP) are $1 - 2\ mm/yr$. The highest basal melt rates (600 mm/yr) occur at the grounding line of Zachariæ, with surface velocities reaching 1500 m/yr. Friction is the dominating heat source in the fast flowing regions, and melt rates thus increase with increasing velocities towards the grounding line. Low melt rates in regions with high velocity are due to low lying bed topography causing low basal drag and hence less frictional heat. The melt rates serve as input to the subglacial hydrology model, and the computed effective pressure, N, is shown in Figure 2k. In the regions where no melt

125   occurs, we prescribe a null water pressure yielding an effective pressure equal to ice overburden pressure. Effective pressure increases upstream toward the ice divide as ice thickness increases and basal melt decreases. The lowest values of N coincide with low bed elevation in the main trunk, 100 km upstream of the grounding line.

    The resulting velocity field for the Ctrl simulation captures the main features of NEGIS: the three outlets with high velocities across the grounding lines and sharp shear margins (Figure 2p). The northern branch feeding into 79N is slower and less

130 defined than in the observed velocities, and the velocities of Storstrømmen are also slower than observed. Velocities of the
floating tongues of 79N and Zachariæ are not well represented, and floating shelves are not shown here. The western branch,
feeding into the main trunk of NEGIS, shows a more diffuse pattern with higher velocities than observed. However, the 50 m/yr
modelled velocity contour, plotted as black lines in Figure 2p, reaches 305 km from the ice divide. This is further downstream
compared to the observed velocity (120 km), plotted as white contours in Figure 2a,f,k. The Ctrl simulation does not capture
135 the characteristics of NEGIS; with high upstream velocities close to the ice divide.

To capture the upstream velocities, we enhance the geothermal heat flux locally at the onset of the ice stream in the plume970
simulation, to reach values proposed by Fahnestock et al. (2001) and Macgregor et al. (2016). The addition of the mantle plume
results in high geothermal heat flux, with values up to $970 \ mW/m^2$, rapidly decreasing to the values used in Ctrl (Figure 2e)
within a radius of less than 100 km. High geothermal heat leads to high basal melt rates, with $100 \ mm/yr$ above the plume
140 (Figure 2j), compared to 1-2 mm/yr in the Ctrl experiment. The increase in basal melt rates is causing a reduction in effective
pressure to 1.2 MPa directly above the plume, resulting in a local floatation fraction (ratio of water pressure over overburden
pressure) of 0.95. The resulting velocity field in the plume970 experiment is similar to the Ctrl experiment, except for the
higher velocities simulated at the head of the ice stream. In the plume970 simulation the $50 \ m/yr$ velocity contour reaches
131 km from the ice divide (black contour Figure 2t), which is close to the observed 120 km. However, the spatial pattern
145 upstream is more diffuse and the ice stream is wider than observed. The Storstrømmen outlet shows higher velocities relative
to the Ctrl, but still lower than observed. The 79N and Zachariæ outlets, on the other hand, display higher velocities than
observed. Overall, with this approach, we capture most of the characteristics of NEGIS, although the ice stream is more diffuse
and displays velocities slightly higher than the observations.

To determine whether a lower geothermal heat flux may induce a similar high velocity pattern, we run three simulations
150 with a less intense mantle plume. Figure 2b-d show the geothermal heat flux values computed by rising the plume depth to
3000, 4000 and 4500 km, respectively, obtaining maximum basal melt rates of 70 (Figure 2g), 85 (Figure 2h) and 95 mm/yr
(Figure 2i). The modelled effective pressure for the three plumes (Figure 2l-n) result in slower velocities than the plume970,
with 50 m/yr velocity contours reaching to 253, 245 and 210 km from the ice divide, respectively (Figure 2q-s). This shows
that GHF values of 677, 836 and $909 \ mW/m^2$ are not sufficient to induce the upstream fast flow of NEGIS.

155 To investigate the sensitivity of the position of the plume in plume970, we moved the plume 75 km to the south-west,
south-east, north-east and north-west (Figure 3). The computed geothermal heat flux distribution is shown in (Figure 3a-d)
and the basal melt rates are of the same magnitude as in the plume970. The computed effective pressure for south-west and
south-east (plume970SW and plume970SE, Figure 3i,j) have minimum values of 3.2 and 2.9 MPa above the plume, which
are not sufficient to initiate fast flow (Figure 3m,n). When the plume is located further downstream, the effective pressure
160 reaches lower values (Figure 3k,l) and the ice stream flows faster than in plume970 (Figure 3o,p). However, with the 50 m/yr
contour only reaching 204 km from the ice divide. The plume970NE induces the fastest flow, and the plume970NW creates
an interesting double branched ice stream starting from the ice divide. The experiments in Figure 3 show that the elevated heat
required to initiate NEGIS must be located close to EGRIP.

To determine whether a lower geothermal heat flux value over a larger area could induce high upstream velocities, we investigate the influence of four weaker plumes with larger plume radii (Figure 4). The weakest, but most extensive plume (plume494, Figure 4a), produces basal melt rates of maximum 51 mm/yr (Figure 4e), resulting in a large area of low effective pressure (minimum 0.2 MPa; Figure 4i). The corresponding surface velocity for the plume494 displays a faster and wider ice stream (Figure 4m) relative to the observations. Plume594 gives basal met rates of 60 mm/yr (Figure 4f) and the ice stream becomes wide, reaching all the way to the ice divide (Figure 4n). The plume775 is twice the size of the plume970 (Figure 4c), and with melt rates of 75 mm/yr over a larger area (Figure 4g), the velocity of the ice stream (Figure 4o) is similar to the plume970. However, the 50 m/yr velocity contour reaches too close to the ice divide and the ice stream is wider than the observed one. The plume792 produces melt rates of 75 mm/yr (Figure 4d), resulting in velocities similar to the plume594 (Figure 4p). This shows that the elevated heat inducing the upstream fast flow of NEGIS must be constrained to a relatively small area, with an extent of ~50 km.

Finally, we investigate the influence of varying the parameters in the friction law (Eq. 1), presented in Figure 5. The noHydro simulation with an effective pressure approximated to the hydrostatic pressure shows very little resemblance to the observed NEGIS (Figure 5a), with too slow velocities. The simulation with a uniform friction coefficient and no mantle plume, captures the main feature of NEGIS (Ctrl-uni, Figure 5b); with a main trunk, the northern branch and three outlets, with fastest flow in Zachariæ. However, the velocity pattern is more diffuse than the observed (Figure 5e). The high upstream velocities are better captured in the simulation with plume970 and a uniform friction (plume970-uni, Figure 5c). For plume970-uni, high velocities reach slightly closer to the ice divide than the plume970, but the velocities of the main trunk are less confined than in experiment plume970 (Figure 5d) and the observations (Figure 5e).

4 Discussion

Most of the spatial velocity pattern of NEGIS is represented in our Ctrl run, apart from the upstream one third of the main trunk. This indicates that the downstream area of the NEGIS catchment is largely controlled by topography, while the upstream area is controlled by its basal conditions, which is in agreement with Keisling et al. (2014). The Ctrl simulation captures the main outlets and the observed "snake" shaped velocity pattern of the trunk. High velocities coincide with low lying bed elevation. However, we do not capture the high velocity of Storstrømmen, or the floating tongues of Zachariæ and 79North outlets. This could be caused by the simple friction coefficient approach not being representative of these areas, where basal properties display a more complex pattern.

We performed experiments with various mantle plume configurations introduced at the head of NEGIS, to assess if the presence of an anomalously high GHF can explain the pattern of ice flow of this region. The different plume configurations vary in intensity, position and extent. In the Ctrl simulation we use present day surface velocity and GHF from Fox Maule et al. (2009). Without the presence of a plume, the GHF does not reach more than $54 \ mW/m^2$ and leads to underestimating velocities in the upstream part of the catchment. These low values of GHF are not sufficient to initiate the onset of NEGIS close to the ice divide. By testing with four mantle plume configurations of increasing intensity (Figure 2), we find that the
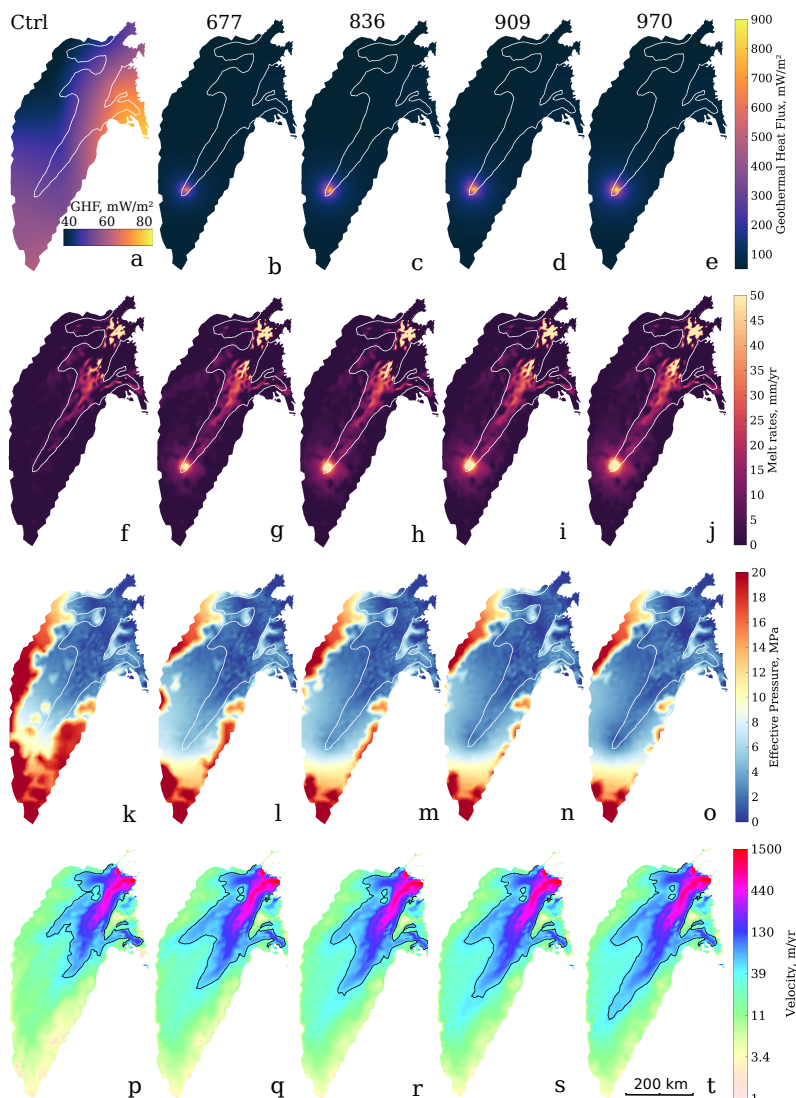
Figure 2. Model results for the Ctrl and the plume677, plume836, plume909 and plume970 simulations. a-e show the modelled geothermal heat flux (note the different color scale for Ctrl) and f-j shows the corresponding basal melt rates, forcing the hydrology model which computes the corresponding effective pressure (k-o) and finally the resulting surface velocity (p-t). White lines show the 50 m/yr observed velocity contour, and black lines show the 50 m/yr modelled velocity contour.

geothermal heat flux (GHF) needed to induce the observed upstream velocity of NEGIS, is $\sim 970 \ mW/m^2$, as proposed by Fahnestock et al. (2001). However, we show that lower values of GHF can induce even faster flow, when the plume is more extensive (Figure 4). However, with a larger mantle plume the ice stream becomes wider, and does not match the observed velocity of NEGIS (Figure 5e), indicating that the heat anomaly initiating NEGIS may be local in extent.
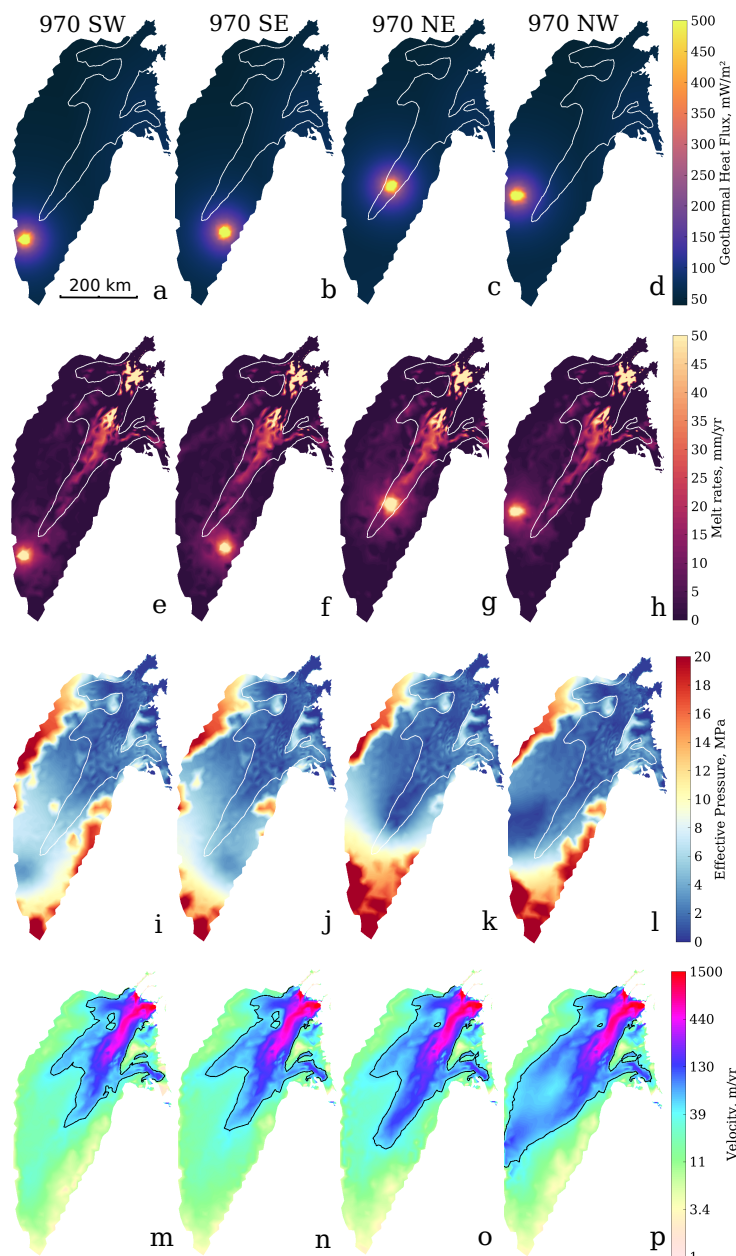
Figure 3. Model results from the sensitivity simulations investigating the position of the mantle plume by moving the plume97 75 km. First column shows results from plume970SW, with a plume 75 km to the south-west, second column represents 970 SE Plume, third represents plume970NE and the last column is plume970NW. a-d show the geothermal heat flux, e-h the resulting basal melt rates, i-l the computed effective pressure and m-p the modelled surface velocity. White lines show the 50 m/yr observed velocity contour, and black lines show the 50 m/yr modelled velocity contour.

By directly comparing the basal melt rates of our plume970 experiment to the basal melt rate estimates from Macgregor et al. (2016), it can be seen that our plume produces a basal melt pattern that matches the position, extent and values of the north-eastern branch of their anomaly (north of the green box in their Figure 5a). This suggest that the onset of NEGIS is triggered by this smaller basal melt anomaly, rather than the larger upstream anomaly reaching all the way to the ice divide (Macgregor
205 et al. (2016), green box in Figure 5a). The sensitivity simulations in Figure 3m,n show that more than 970 mW/m^2 is needed to initiate high velocity, when the plume is located further upstream in a region with thicker ice relative to downstream. Thus, the larger upstream anomaly in Macgregor et al. (2016) may have less impact on the dynamics of the NEGIS.

To capture the observed upstream velocities we have forced the model with an extremely high GHF value (970 mW/m^2), ten times higher than the values suggested for Greenland (Rogozhina et al., 2012; Shapiro and Ritzwoller, 2004; Fox Maule
210 et al., 2009; Martos et al., 2018; Rogozhina et al., 2016). The required heat flux is three times as high as the highest geothermal heat flux observations in Greenland (Rysgaard et al., 2018). However, it is 300 times less than estimated under Myrdalsjokull in Iceland (Jarosch and Gudmundsson, 2007). 970 mW/m^2 is only applied to one node in our model mesh, and the values are rapidly decreasing to less than half within a radius of 25 km. The magnitude of the anomaly corresponds to the values suggested by Fahnestock et al. (2001). Greve (2019) derived GHF values for five deep ice core bore holes in Greenland,
215 using the SICOPOLIS model (SImulation COde for POLythermal Ice Sheets; www.sicopolis.net), such that the simulated and observed basal temperatures match. This resulted in a local elevated GHF anomaly around NGRIP of 135 mW/m^2, located at the ice divide $\sim 150\ km$ away from the head of NEGIS. Our GHF anomaly is smaller in extent, and with a magnitude 7 times higher than Greve (2019). The large difference in magnitude may be due to the very different constraints; Greve (2019) uses observed basal temperatures, and we use observed velocities as a target.

220 Local high heat flux does not come from variations in the mantle, but local variations in the crustal heat production and possibly hydrothermal systems. We are not suggesting a mantle plume to be present beneath NEGIS, rather the high values are reminiscent of previously high values from the passage of Greenland over the Iceland Plume. However, we represent the potential extra heat source using the mantle plume module in ISSM. Alley et al. (2019) and Stevens et al. (2016) explained high GHF in this region by the passing of the Iceland plume, leaving behind partly molten rock that may have migrated up
225 in response to glacial-interglacial cycles, as the crust is loaded and unloaded. The plume passage could have lead to shallow magma emplacements, that may feed hydrothermal systems, causing hot fluid percolation that enhances high heat transport to the base of the ice sheet (Stevens et al., 2016; Alley et al., 2019). The mantle plume passed across Greenland, however, abnormally high melt rates are only found at the onset of NEGIS (Macgregor et al., 2016). This could be due local lithology, causing rifts or other weaknesses in the continental plate during glacial rebound, making this region unique. A study showed
230 that glacial rebound may have caused young intraplate volcanism in Greenland, despite the old age of the tectonic plate and no mantle plume present (Uenzelmann-Neben et al., 2012).

Comparing the velocity field in the plume970 experiment to previous studies without inversion shows that combining a basal hydrology model with an elevated GHF at the head of NEGIS captures the observed high, confined, upstream velocities of the NEGIS. The simulations in Goelzer et al. (2018) show that the ice flow models capturing the upstream onset of NEGIS all rely
235 on inversions to initialize the basal drag in the simulations (Elmer/Ice, ISSM, BISICLES, GRISLI and f.Etish). The models

without inversion, underestimate the velocities in the upper part of NEGIS catchment and lack the sharp velocity gradients. Aschwanden et al. (2016) simulated the high upstream velocity of NEGIS without inverting for basal conditions in PISM, but their simulation lacks the clearly defined main trunk and underestimates the high upstream velocity. Beyer et al. (2018) further improved the simulation by using a subglacial hydrology model to compute effective pressure, which allowed higher velocities

240 in the outlets. However, high upstream velocities are still lacking, similar to our Ctrl simulation. The two latter studies used GHF from Shapiro and Ritzwoller (2004), which proposed slightly lower values at the head of NEGIS compared to the values of Fox Maule et al. (2009) used in our study.

Beyer et al. (2018) used the same friction law as we use in ISSM, but with a uniform friction coefficient. We tested a uniform friction coefficient, which lead to a more diffuse ice stream (Figure 5b,c), but with more confined outlets compared to the Beyer

245 et al. (2018) study. The difference can be explained by different basal melt rates used as input, and different hydrology models. In order to capture sharp gradients in the velocity field, we find it important that the areas without any basal melt have effective pressure equal to the ice overburden pressure.

We invert for basal friction to get the basal melt rates that are used to initialize the subglacial hydrology model, and the model is then free to evolve. We do not use the inverted friction in the forward ice flow simulation, instead we use the simple friction

250 coefficient from Eq. 2. To investigate whether the modelled velocity pattern is caused by the effective pressure distribution or the friction coefficient, we run the simulation 'no Hydro', where the effective pressure is approximated to the hydrostatic pressure, commonly used in ISSM. The modelled velocity pattern (Figure 5a) does not resemble the observed, and we conclude that including the subglacial hydrology model is responsible for the improved velocity pattern in Ctrl and plume970. By using our friction coefficient distribution, combined with initializing with present-day basal melt from velocity observations, both

255 the Ctrl and plume970 experiments display velocity patterns similar to the observations (Figure 5d,e).

The middle western branch of the ice stream displays too high velocity in both the Ctrl and plume970 experiments, correlating with low lying bed elevation (Figure 1). Too high velocities in this region were also modelled by Aschwanden et al. (2016) using PISM and a similar bed elevation dependent friction law. When performing additional simulations with the GHF values from Martos et al. (2018) this branch becomes more pronounced in velocity (not shown here). This may indicate that the

260 GHF values in this region of Greenland are even lower than Martos et al. (2018) and Fox Maule et al. (2009), and the glacier base is frozen to the ground. This region is recognized as "uncertain" in the synthesis of Greenland's basal thermal regime by Macgregor et al. (2016). Other explanations for too high velocities in this branch may be a higher bed roughness, errors in the bed topography or "sticky spots".

Given the model configuration, an exceptionally high GHF value of $970\ mW/m^2$ is needed to reproduce NEGIS. Hydrology

265 parameters are unfortunately highly uncertain, and different choices would lead to a more or less responsive hydrological system. However, we have a rather low transmissivity of the inefficient drainage system, resulting in low efficiency in water evacuation, causing our system to be sensitive to an increase in water input. If the transmissivity was lowered further, the efficient drainage system is likely to activate in the GHF anomaly region, lowering the water pressure and becoming less sensitive to increased water input. For this reason, we do not expect that a different hydrology configuration would reproduce

270 NEGIS with a lower GHF value. In addition, the subglacial hydrology is only one-way coupled to ice dynamics, so we do

not capture the positive feedback expected with higher velocities leading to more melt, and lower effective pressure, giving even higher velocities. With a more responsive and fully coupled system, one might be able to reproduce NEGIS with lower values for the geothermal heat flux. We use a simple friction law linearly dependent on effective pressure, and are aware that the results are likely to change with a different choice of friction law. For example, in the friction law used in the MISMIP+

275 experiments (Asay-Davis et al., 2016; Tsai et al., 2015), effective pressure is included only where the coulomb criterion is met, normally a few km upstream of the grounding line. This may result in a smaller dynamic response from the mantle plume in the slow upstream regions of NEGIS.

With a simple bed elevation dependent friction and hydrology model forced by melt rates from GHF, we capture the overall pattern of NEGIS velocity. This has implications for studies trying to predict the response of NEGIS to a future climatic

280 warming. Basal friction may not remain constant in time, and thus we cannot fully rely on inversion as it masks unknown time varying basal properties. By using our approach (with or without the geothermal heat flux anomaly) one can capture complex velocity patterns, and then invert for the remaining basal properties. These may in turn be assumed to be constant in time, while the subglacial hydrology will evolve with a changing climate accounting for varying basal conditions. Unfortunately, observations and estimates of geothermal heat flux and subglacial hydrology are challenged by large uncertainties. Therefore,

285 it is critical for future observational and modelling studies, to better constrain the basal conditions of the Greenland Ice Sheet.

5 Conclusions

Present day basal melt rates from geothermal heat flux maps and frictional heat are not sufficient to sustain the observed upstream velocities of Northeast Greenland Ice Stream (NEGIS), as opposed to the downstream velocities which appear to be driven by topography. Our findings suggest that a local geothermal heat flux anomaly may explain the characteristic high

290 upstream velocity of NEGIS, and hence confirms previous studies (Fahnestock et al., 2001; Macgregor et al., 2016; Alley et al., 2019). To reproduce high upstream velocities at the onset of NEGIS, a sustained basal melt rate of $100 \ mm/yr$ is needed in a local region close to EastGRIP where observed present day velocities reach 50 m/yr. Hence, the minimal geothermal heat flux value needed to initiate the ice stream in our model is $970 \ mW/m^2$, as proposed by Fahnestock et al. (2001).

Code and data availability. ISSM software is open source and can be downloaded at https://issm.jpl.nasa.gov/. The surface mass balance

295 forcing used in this study, from J.E. Box, is available from https://zenodo.org/record/3359192#.XUSmSpNKhR4 (Box, 2019).

Author contributions. SSJ designed the study with help from BdF and KHN. SSJ ran the simulations. NS helped greatly setting up the ice flow model, BdF helped setting up the hydrology model, and HS helped setting up the mantle Plume model. SSJ wrote the manuscript with substantial contributions from all co-authors. The research related to the paper was discussed by all co-authors.

Competing interests. The authors declare that they have no conflict of interest.

300   *Acknowledgements.* SSJ, BdF and KHN were funded by the Ice2Ice project that has received funding from the European Research Council under the European Community's Seventh Framework Programme (FP7/2007-2013)/ERC grant agreement No. 610055. BdF is also funded by SWItchDyn NRC grant(287206). Funding for HS and NS were provided by grants from NASA Cryospheric Science and Modeling, Analysis and Prediction (MAP) Programs.

References

305   Åkesson, H., Morlighem, M., Nisancioglu, K., Svendsen, J., and Mangerud, J.: Atmosphere-driven ice sheet mass loss paced by topography: Insights from modelling the south-western Scandinavian Ice Sheet, Quaternary Science Reviews, 195, 32–47, https://doi.org/10.1016/j.quascirev.2018.07.004, 2018.

Alley, R. B., Pollard, D., Parizek, B. R., Anandakrishnan, S., Pourpoint, M., Stevens, N. T., MacGregor, J., Christianson, K., Muto, A., and Holschuh, N.: Possible Role for Tectonics in the Evolving Stability of the Greenland Ice Sheet, Journal of Geophysical Research: Earth
310   Surface, pp. 1–19, https://doi.org/10.1029/2018JF004714, 2019.

Asay-Davis, X. S., Cornford, S. L., Durand, G., Galton-Fenzi, B. K., Gladstone, R. M., Gudmundsson, G. H., Hattermann, T., Holland, D. M., Holland, D., Holland, P. R., Martin, D. F., Mathiot, P., Pattyn, F., and Seroussi, H.: Experimental design for three interrelated marine ice sheet and ocean model intercomparison projects: MISMIP v. 3 (MISMIP +), ISOMIP v. 2 (ISOMIP +) and MISOMIP v. 1 (MISOMIP1), Geoscientific Model Development, 9, 2471–2497, https://doi.org/10.5194/gmd-9-2471-2016, 2016.

315   Aschwanden, A., Bueler, E., Khroulev, C., and Blatter, H.: An enthalpy formulation for glaciers and ice sheets, Journal of Glaciology, 58, 441–457, https://doi.org/10.3189/2012JoG11J088, 2012.

Aschwanden, A., Fahnestock, M., and Truffer, M.: Complex Greenland outlet glacier flow captured, Nature Communications, 7, https://doi.org/10.1038/ncomms10524, 2016.

Beyer, S., Kleiner, T., Aizinger, V., and Humbert, A.: A confined–unconfined aquifer model for subglacial hydrology and its application to
320   the North East Greenland Ice Stream, The Cryosphere Discussions, pp. 1–24, 2018.

Box, J.: Greenland monthly surface mass balance 1840-2012, https://doi.org/5281/zenodo.3359192, 2019.

Cooper, M. A., Jordan, T. M., Schroeder, D. M., Siegert, M. J., Williams, C. N., and Bamber, J. L.: Subglacial roughness of the Greenland Ice Sheet: relationship with contemporary ice velocity and geology, The Cryosphere Discussions, pp. 1–38, https://doi.org/10.5194/tc-2019-73, 2019.

325   Cuffey, K. M. and Paterson, W. S. B.: The physics of glaciers, Academic Press, 2010.

Cuzzone, J. K., Morlighem, M., Larour, E., Schlegel, N., and Seroussi, H.: Implementation of higher-order vertical finite elements in ISSM v4.13 for improved ice sheet flow modeling over paleoclimate timescales, Geoscientific Model Development, 11, 1683–1694, https://doi.org/10.5194/gmd-11-1683-2018, 2018.

de Fleurian, B., Gagliardini, O., Zwinger, T., Durand, G., Le Meur, E., Mair, D., and Räback, P.: A double continuum hydrological model for
330   glacier applications, Cryosphere, 8, 137–153, https://doi.org/10.5194/tc-8-137-2014, 2014.

de Fleurian, B., Morlighem, M., Seroussi, H., Rignot, E., van den Broeke, M. R., Kuipers Munneke, P., Mouginot, J., Smeets, P. C. P., and Tedstone, A. J.: A modeling study of the effect of runoff variability on the effective pressure beneath Russell Glacier, West Greenland, Journal of Geophysical Research: Earth Surface, 121, 1834–1848, https://doi.org/10.1002/2016JF003842, 2016.

Ettema, J., Bales, R. C., Box, J. E., van Meijgaard, E., van den Broeke, M. R., van de Berg, W. J., and Bamber, J. L.: Higher sur-
335   face mass balance of the Greenland ice sheet revealed by high-resolution climate modeling, Geophysical Research Letters, 36, 1–5, https://doi.org/10.1029/2009gl038110, 2009.

Fahnestock, M., Abdalati, W., Joughin, I., Brozena, J., and Gogineni, P.: High Geothermal Heat Flow, Basal Melt, and the Origin of Rapid Ice Flow in Central Greenland, Science, 294, 2338–2342, 2001.

Fox Maule, C., Purucker, M. E., and Olsen, N.: Inferring magnetic crustal thickness and geothermal heat flux from crustal magnetic field
340   models, November, 2009.

Goelzer, H., Nowicki, S., Edwards, T., Beckley, M., Abe-Ouchi, A., Aschwanden, A., Calov, R., Gagliardini, O., Gillet-Chaulet, F., Golledge, N., Gregory, J., Greve, R., Humbert, A., Huybrechts, P., Kennedy, J., Larour, E., Lipscomb, W., Leclech, S., Lee, V., Morlighem, M., Pattyn, F., Payne, A., Rodehacke, C., Rückamp, M., Saito, F., Schlegel, N., Seroussi, H., Shepherd, A., Sun, S., Van De Wal, R., and Ziemen, F.: Design and results of the ice sheet model initialisation initMIP-Greenland: An ISMIP6 intercomparison, Cryosphere, 12, 1433–1460, https://doi.org/10.5194/tc-12-1433-2018, 2018.

Greve, R.: Geothermal heat flux distribution for the Greenland ice sheet, derived by combining a global representation and information from deep ice cores, Polar Data, 3, 2019.

Jarosch, A. H. and Gudmundsson, M. T.: Numerical studies of ice flow over subglacial geothermal heat sources at Grimsvatn, Iceland, using Full Stokes equations, Journal of Geophysical Research: Earth Surface, 112, 1–10, https://doi.org/10.1029/2006JF000540, 2007.

Keisling, B., Christianson, K., Alley, R. B., Peters, L. E., Christian, J. E. M., Anandakrishnan, S., Riverman, K. L., Muto, A., and Jacobel, R. W.: Basal conditions and ice dynamics inferred from radar-derived internal stratigraphy of the northeast Greenland ice stream, Annals of Glaciology, 55, 127–137, https://doi.org/10.3189/2014AoG67A090, 2014.

Khroulev, C. and PISM-Authors: PISM, a Parallel Ice Sheet Model: User's Manual, 408, 2015.

Larour, E., Seroussi, H., Morlighem, M., and Rignot, E.: Continental scale, high order, high spatial resolution, ice sheet modeling using the Ice Sheet System Model (ISSM), Journal of Geophysical Research: Earth Surface, 117, F01 022, https://doi.org/10.1029/2011JF002140, 2012.

Macgregor, J., Fahnestock, M., Catania, G., Aschwanden, A., Clow, G., Colgan, W., Gogineni, S., Morlighem, M., Nowicki, S., Paden, J., Price, S., and Seroussi, H.: A synthesis of the basal thermal state of the Greenland Ice Sheet, Journal of Geophysical Research: Earth Surface, pp. 1328–1350, https://doi.org/10.1002/2015JF003803, 2016.

Martos, Y. M., Jordan, T. A., Catalan, M., Jordan, T. M., Bamber, J. L., and Vaughan, D. G.: Geothermal heat flux reveals the Iceland hotspot track underneath Greenland, Geophysical Research Letters, https://doi.org/10.1029/2018GL078289, 2018.

Morlighem, M., Seroussi, H., Larour, E., and Rignot, E.: Inversion of basal friction in Antartica using exact and incomplete adjoints of a higher-order model, Journal of Geophysical Research: Earth Surface, 118, 1746–1753, https://doi.org/10.1002/jgrf.20125, 2013.

Morlighem, M., Rignot, E., Mouginot, J., Seroussi, H., and Larour, E.: Deeply incised submarine glacial valleys beneath the Greenland ice sheet, Nature Geoscience, 7, 18–22, https://doi.org/10.1038/ngeo2167, 2014.

Pattyn, F.: A new three-dimensional higher-order thermomechanical ice sheet model: Basic sensitivity, ice stream development, and ice flow across subglacial lakes, Journal of Geophysical Research, 108, 2382, https://doi.org/10.1029/2002JB002329, 2003.

Rignot, E. and Mouginot, J.: Ice flow in Greenland for the International Polar Year 2008-2009, Geophysical Research Letters, 39, 1–7, https://doi.org/10.1029/2012GL051634, 2012.

Rignot, E., Gogineni, S., Joughin, I., and Krabill, W.: Contribution to the glaciology of nothern Greenland from satellite radar interferometry, Journal of Geophysical Research, 106, 34 007–34 019, 2001.

Rogozhina, I., Hagedoorn, J. M., Martinec, Z., Fleming, K., Soucek, O., Greve, R., and Thomas, M.: Effects of uncertainties in the geothermal heat flux distribution on the Greenland Ice Sheet: An assessment of existing heat flow models, Journal of Geophysical Research, 117, 1–16, https://doi.org/10.1029/2011JF002098, 2012.

Rogozhina, I., Petrunin, A. G., Vaughan, A. P. M., Steinberger, B., Johnson, J. V., Kaban, M. K., Calov, R., Rickers, F., Thomas, M., and Koulakov, I.: Melting at the base of the Greenland ice sheet explained by Iceland hotspot history, Nature Geoscience, 9, 366–369, https://doi.org/10.1038/ngeo2689, 2016.

Rysgaard, S., Bendtsen, J., Mortensen, J., and Sejr, M. K.: High geothermal heat flux in close proximity to the Northeast Greenland Ice Stream, Scientific Reports, 8, 1–8, https://doi.org/10.1038/s41598-018-19244-x, 2018.

380 Schlegel, N. J., Larour, E., Seroussi, H., Morlighem, M., and Box, J. E.: Decadal-scale sensitivity of Northeast Greenland ice flow to errors in surface mass balance using ISSM, Journal of Geophysical Research: Earth Surface, 118, 667–680, https://doi.org/10.1002/jgrf.20062, 2013.

Schlegel, N.-J., Larour, E., Seroussi, H., Morlighem, M., and Box, J. E.: Ice discharge uncertainties in Northeast Greenland from climate forcing and boundary conditions of an ice flow model, Journal of Geophysical Research: Earth Surface, submitted, 1–21,
385 https://doi.org/10.1002/2014JF003359.Received, 2015.

Seroussi, H., Morlighem, M., Rignot, E., Khazendar, A., Larour, E., and Mouginot, J.: Dependence of century-scale projections of the Greenland ice sheet on its thermal regime, Journal of Glaciology, 59, 1024–1034, https://doi.org/10.3189/2013JoG13J054, 2013.

Seroussi, H., Ivins, E. R., Wiens, D. A., and Bondzio, J.: Influence of a West Antarctic mantle plume on ice sheet basal conditions, Journal of Geophysical Research: Solid Earth, 122, 7127–7155, https://doi.org/10.1002/2017JB014423, 2017.

390 Shapiro, N. M. and Ritzwoller, M. H.: Inferring surface heat flux distributions guided by a global seismic model: Particular application to Antarctica, Earth and Planetary Science Letters, 223, 213–224, https://doi.org/10.1016/j.epsl.2004.04.011, 2004.

Smith-Johnsen, S., de Fleurian, B., and Nisancioglu, K.: The role of subglacial hydrology in ice streams with elevated geothermal heat flux, Journal of Glaciology, in reviewa.

Smith-Johnsen, S., Schlegel, N.-J., de Fleurian, B., and Nisancioglu, K.: Sensitivity of the Northeast Greenland Ice Stream to Geothermal
395 Heat, Journal of Geophysical Research: Earth Surface, in reviewb.

Stevens, N. T., Parizek, B. R., and Alley, R. B.: Enhancement of volcanism and geothermal heat flux by ice-age cycling: A stress modeling study of Greenland, pp. 1456–1471, https://doi.org/10.1002/2016JF003855.Received, 2016.

Tsai, V. C., Stewart, A. L., and Thompson, A. F.: Marine ice-sheet profiles and stability under Coulomb basal conditions, Journal of Glaciology, 61, 205–215, https://doi.org/10.3189/2015JoG14J221, 2015.

400 Uenzelmann-Neben, G., Schmidt, D. N., Niessen, F., and Stein, R.: Intraplate volcanism off South Greenland: Caused by glacial rebound?, Geophysical Journal International, 190, 1–7, https://doi.org/10.1111/j.1365-246X.2012.05468.x, 2012.
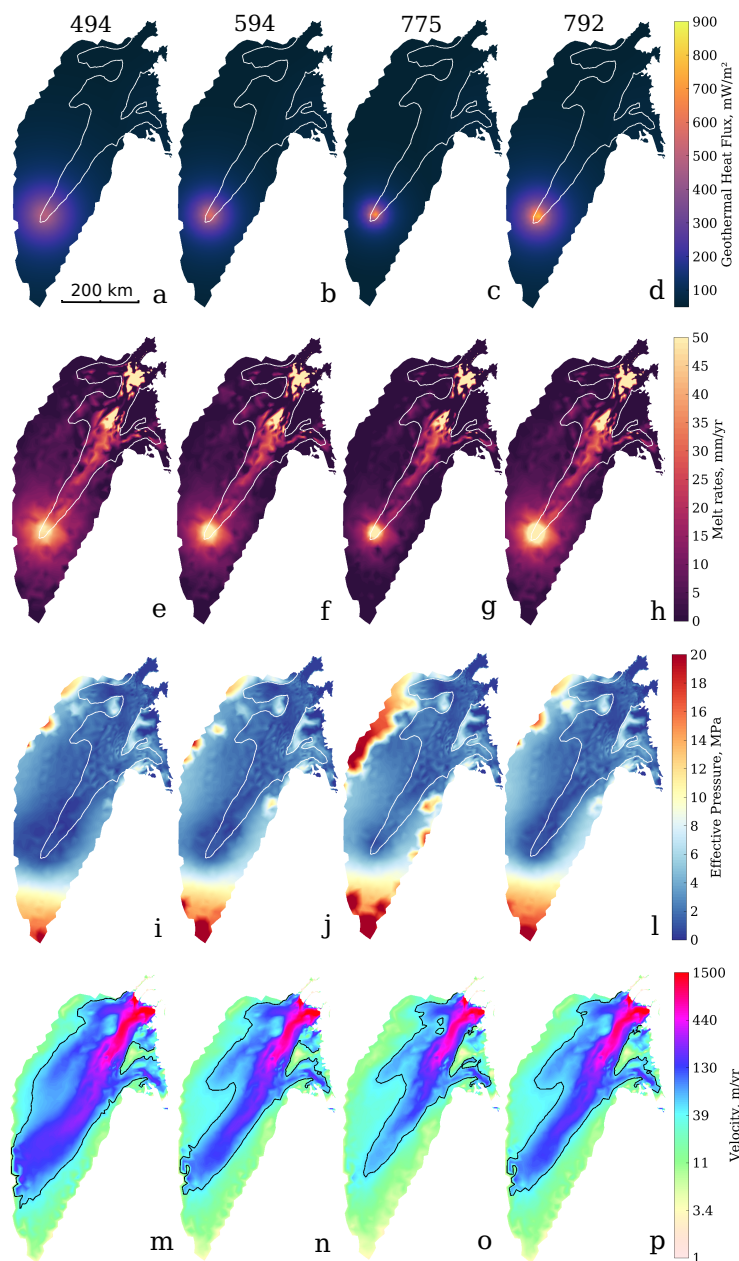
Figure 4. Model results from the sensitivity simulations investigating a reduced magnitude and increased size of the mantle plume. First column shows results from 494 Plume with a 300 km radius at 3000 km depth, second column represents 594 Plume with 200 km radius and 2500 km depth, third column represents 775 Plume with 100 km radius and 2000 km depth the last column represents Plume 792 with 200 km radius and 3000 km depth. a-d show the geothermal heat flux, e-h the resulting basal melt rates, i-l the compute effective pressure and m-p the modelled surface velocity. White lines show the 50 m/yr observed velocity contour, and black lines show the 50 m/yr modelled velocity contour.
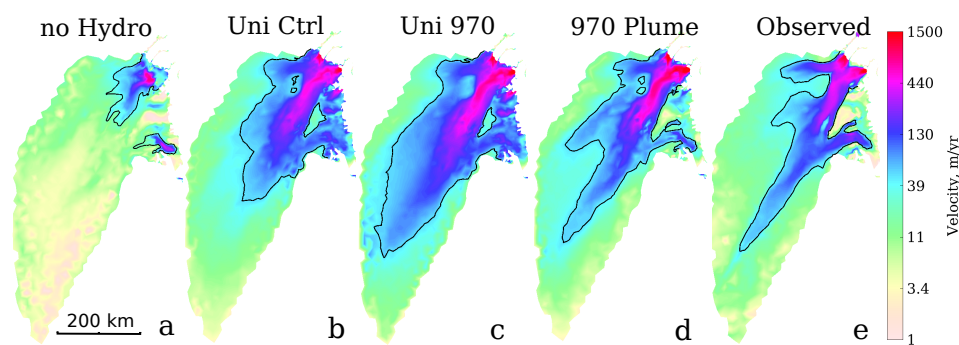
Figure 5. Surface velocity results from the no Hydro (a) with effective pressure approximated to the hydrostatic pressure assuming direct connection to the ocean, commonly used in ISSM. Uni Ctrl (b) and plume970-uni experiment (c) use a uniform friction coefficient α set equal to $90 \ (m/s)^{1/2}$. Corresponding geothermal heat flux, basal melt rates and effective pressure are the same as Ctrl and plume970, shown in Figure 2. For reference we include d showing the plume970 simulation (same as Figure 2t), and e showing the observed surface velocities interpolated onto the model mesh. Black lines show the 50 m/yr velocity contour.